

On the Consistency and Robustness of Saliency Explanations for Time Series Classification

Chiara Balestra*

TU Dortmund
Germany
chiara.balestra@tu-dortmund.de

Bin Li*

TU Dortmund
Germany
bin.li@tu-dortmund.de

Emmanuel Müller

TU Dortmund
Germany
emmanuel.mueller@tu-dortmund.de

ABSTRACT

Interpretable machine learning and explainable artificial intelligence have become essential in many applications. The trade-off between interpretability and model performance is the traitor to developing intrinsic and model-agnostic interpretation methods. Although model explanation approaches have achieved significant success in vision and natural language domains, explaining time series remains challenging. The complex pattern in the feature domain, coupled with the additional temporal dimension, hinders efficient interpretation. Saliency maps have been applied to interpret time series windows as images. However, they are not naturally designed for sequential data, thus suffering various issues.

This paper extensively analyzes the consistency and robustness of saliency maps for time series features and temporal attribution. Specifically, we examine saliency explanations from both perturbation-based and gradient-based explanation models in a time series classification task. Our experimental results on five real-world datasets show that they all lack consistent and robust performances to some extent. By drawing attention to the flawed saliency explanation models, we motivate to develop consistent and robust explanations for time series classification.

CCS CONCEPTS

• **Computing methodologies** → **Machine learning**.

KEYWORDS

Time series, Robustness, Consistency, Explainable machine learning, Saliency maps

ACM Reference Format:

Chiara Balestra, Bin Li, and Emmanuel Müller. 2018. On the Consistency and Robustness of Saliency Explanations for Time Series Classification. In *Proceedings of Make sure to enter the correct conference title from your rights confirmation email (Conference acronym 'XX)*. ACM, New York, NY, USA, 8 pages. <https://doi.org/XXXXXXXX.XXXXXXX>

*Both authors contributed equally to this research.

Permission to make digital or hard copies of all or part of this work for personal or classroom use is granted without fee provided that copies are not made or distributed for profit or commercial advantage and that copies bear this notice and the full citation on the first page. Copyrights for components of this work owned by others than ACM must be honored. Abstracting with credit is permitted. To copy otherwise, or republish, to post on servers or to redistribute to lists, requires prior specific permission and/or a fee. Request permissions from permissions@acm.org.
Conference acronym 'XX, June 03–05, 2018, Woodstock, NY
© 2018 Association for Computing Machinery.
ACM ISBN 978-1-4503-XXXX-X/18/06...\$15.00
<https://doi.org/XXXXXXXX.XXXXXXX>

1 INTRODUCTION

The spread of machine learning techniques to safety-critical applications has raised major concerns about model interpretability. Although shallow models are inherently easily interpretable and broadly applied, they often lack accuracy compared to more sophisticated prediction models whose predictions' interpretation is far from obvious. This trade-off between interpretability and model performance has increased the interest in post-hoc explanations techniques, ideally model-agnostic, straightforward, and robust. Saliency explanation recently gained traction and succeeded in various computer vision [16, 20] and natural language processing tasks [18, 26]; However, explaining time series models still faces challenges. Saliency maps provide pixel importance scores that can be easily interpreted, visually identifying the most relevant areas for the given task; A notable example is image classification, where saliency maps can visually highlight influential areas to the predicted label, making them valuable methods for explaining predictions. The importance scores are assigned using various techniques and are mainly divided into gradient-based and perturbation-based methods. Additionally, Shapley values do not fall into these two categories but provide one approach to getting saliency maps. The structure of time series data has generated interest in directly applying saliency maps to obtain meaningful explanations for classification models [8]. However, images and time series represent fundamentally different types of data. On the one hand, the temporal dependency in time series leads to time-dependent changes in feature attribution. On the other hand, explanation approaches are often not directly applicable to time series models with recurrent- or attention-based components [5, 9]. Although several approaches try to treat data windows of time series as images and apply vision explanation methods [8, 15], the quality of such explanations is often questionable. We address two main issues that arise when using saliency maps for explaining time series data predictions; We introduce two concerns, i.e., the *consistency* and the *robustness* of saliency maps on time series, and show in the experiments that the typical attribution approaches used for time series are neither robust nor consistent.

Deep time series analysis models usually consider sliding windows as basic input units to capture temporal information. Analog to saliency maps for visualizing image pixel importance, similar saliency maps are generated for time series frames with *feature-time pixel* importance. Current research on explanation approaches for time series data can be classified into two categories. The first category contains methods treating sliding windows as *frames* of images and applying classical image explanation methods, e.g., SHAP [14], LIME [17], and DeepLIFT [20]. Those methods extract local feature information while disregarding the time structure typical of the time series data. The second category contains methods considering the

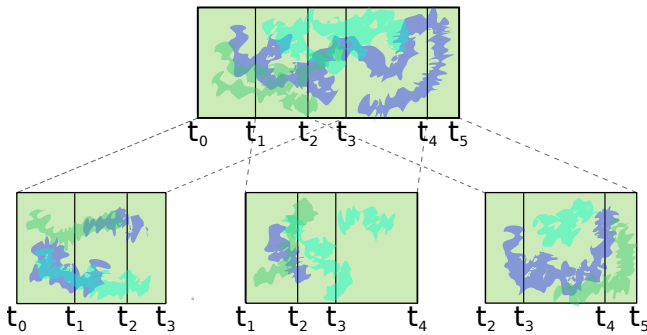


Figure 1: Representation of inconsistencies among saliency maps of adjacent sliding windows (x -axis: time, y -axis: features, color: importance attribution). The saliency map in the top shows overall attribution from t_0 to t_5 . The bottom row shows the saliency maps relative to three adjacent sliding windows (from left to right, in the interval $[t_0, t_3]$, $[t_1, t_4]$ and $[t_2, t_5]$). It is easy to spot that the color distributions in the overlapping window $[t_2, t_3]$ in the four cases are different.

time dimension as an additional feature for joint explanation [3, 8]. Overall, explanation methods on time series data consider the time dimension either jointly with the other features [15] or separately [8], through sequentially considering time and features. In both cases, the explanation is limited to one single *frame* (i.e., sliding window). Hence, both categories reveal insufficient for interpreting the overall temporal information over a long time span. We claim that explanations over the intersection of sliding windows should exhibit *consistent* behaviors to identify such a flaw in current time series saliency explanations. We admit that in adjacent sliding windows, different temporal contexts may lead to different absolute feature attribution. Therefore, we pursue *consistency* relative attribution in local sub-windows. Figure 1 illustrates the meaning of *consistency* among overlapping time windows.

In addition to the saliency explanation consistency, the robustness of saliency maps against feature perturbation is another essential factor in ensuring explanation quality. In images, the semantic meaning of columns and rows is equivalent, while in time series, the time structure makes time series data semantically different and introduces dependence among the observations in the various timestamps; In images, swaps of both rows and columns of pixels affect the semantic structure of the original data, while in time series, only the swaps affecting the temporal orders of the observations are semantically meaningful. In contrast, the order in which input values are collected has no effects. The phenomenon is illustrated in Figure 2 where the x -axis corresponds to the time, and the y -axis to the input variables. When saliency maps are applied to time series, the salient features should be insensitive to the order of input features. When feature columns in the time series frame are swapped, important areas in the saliency map should stay salient in the corresponding swapped areas. We call this the *robustness* of saliency explanation.

This paper studies the *consistency* and *robustness* of saliency explanation in the time series classification task. We examine saliency explanations from popularly used perturbation- and gradient-based approaches [24, 25] on multiple deep classification models [7, 13,

27]. We show on five real-world datasets that the studied saliency explanation suffers from consistency and robustness issues. These preliminary results underline the encountered problems as a motivating example of further research on developing robust and consistent saliency explanations for time series.

2 RELATED WORK

Intrinsic and post-hoc explanations have transformed into a core topic for machine learning research; The interest in increasing the explainability of the methods embraces the entire Machine Learning and AI communities [20, 23]. Gradient (GRAD) was introduced in Baehrens et al. [2] in 2010 as a post-hoc model agnostic interpretation tool able to explain nonlinear classifiers at a local level; The provided explanations measure how each data point has to be moved to change the predicted label [2]. The local scores derive from the direct computation of the local gradients (or their estimations) for the given model. Similarly, Integrated Gradients [24] is also a gradient-based feature importance attribution method and builds up on [2] and two axioms, i.e., the *sensitivity* and *implementation invariance*. Finally, SHAP [14] represents a successful attempt to introduce Shapley values in machine learning; Lundberg et al. [14] use Shapley values to assign importance scores to features for local explanations of black-box models’ predictions; The Shapley values’ approximations are based on the computations of the gradient of the model predictions.

Although progress is not neglectable, the explanations provided by the most recent works are mostly not quantitatively evaluable, thus still raising trust issues in users [29]. Few recent works focus on the quality of the explanation methods; Dombrowski et al. [6] showed that explanations for image classification are non-robust against possible visually hardly detectable manipulations.

Explanation methods appear for most of the machine learning techniques with different strengths. Time series represents one niche data type where most implemented methods still lack explanations. One of the reasons for the poor literature on the explainability of time series data is the additional time-dependent structure. Explanations often reduce to applications of model-agnostic post-hoc explanations for general data samples to time-dependent data; The time structure is often disregarded, and the timestamps are treated as independent samples on which the model is learned [3, 19]. Another thread of approaches using attention-based models obtains time-dependent explanations by attention weights [5, 10, 22]. The acquired feature and time attribution to the prediction can be visualized in saliency maps, which are initially implemented for images [1], and are a current trend in obtaining explanations for importance scores of timestamps and features; Among them, we find gradient-based [2, 20, 21, 24] and perturbation-based feature importance scores [25, 28]. Ismail et al. [8] pointed out how these methods often suffer from a lack of understanding of the time-features structures, either allowing to achieve only good performances at a time level or the features level; The authors propose an alternative two-step approach to saliency explanations for time series, where the time structure is first considered, and the importance of the features are considered only in the second step. The explanation quality of such a method is still under-studied in the time series domain.

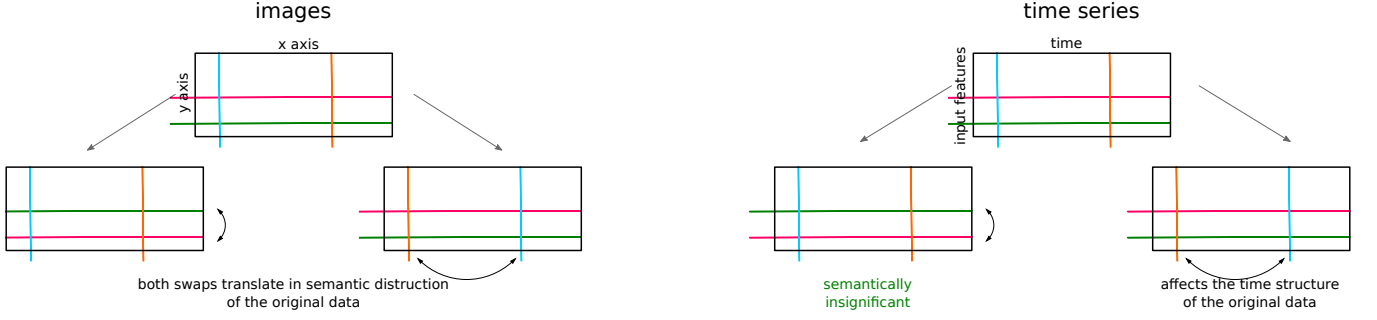


Figure 2: Representative drawings of time series data as 2D data frames. The position of a pixel in an image is defined by row and column numbers, while in time series data, by input variables and timestamps. Swaps of rows and columns of pixels in images may affect the semantic meaning of the entire data frame; For time series, this may happen only when swapping observations at different timestamps.

3 OPEN ISSUES ON SALIENCY EXPLANATIONS

This section formally defines the consistency and robustness of the saliency explanation for time series classification.

We indicate with $X = (X_1, \dots, X_N)$ a multivariate N -dimensional discrete time series where X_i is the i -th univariate dimension; t_0 is the first timestamp on which the time series is defined. For each timestamp $t_k > t_0$, $X(t_k)$ is a N -dimensional vector of real values, i.e., $X(t_k) \in \mathbb{R}^N$. We study the consistency and robustness of saliency explanations for classification models trained on time series data. We draw upon the concept of *consistency* proposed by Pillai et al. [16], and define *consistency* of saliency explanations over adjacent sliding windows of time series. Additionally, regarding *robustness*, we consider the influence of swaps of *features*, i.e., of input variables observations, in explanations using saliency maps.

3.1 Consistency

We define *time windows* $\{w_s^d\}_{s \in \mathbb{N}}$ dependent on the window length $d \in \mathbb{N}$ and the starting timestamp t_s , i.e.,

$$w_s^d = \{t_s, \dots, t_{s+d-1}\}. \quad (1)$$

For each time window and given a fixed saliency map method assignment of importance score S , we get $S(w_s^d) = S_s^d$ a matrix in $\mathbb{R}^{N \times d}$ such that $(S_s^d)_{n,t}$ is the importance scores assigned to the input variable X_n at time t . Saliency maps are transposed from image (pre)processing applications to explain time series classification predictions. We examine the consistency of saliency maps defined over overlapping windows. Given two windows w_s^d and $w_{\bar{s}}^d$ such that $|w_s^d \cap w_{\bar{s}}^d| \neq \emptyset$ and the respective saliency maps S_s^d and $S_{\bar{s}}^d$, the saliency explanations are inconsistent at timestamp t , if $t, \bar{t} \in w_s^d \cap w_{\bar{s}}^d$ such that

$$(S_s^d)_{n,t} > (S_{\bar{s}}^d)_{n,t} \text{ and } (S_s^d)_{n,\bar{t}} < (S_{\bar{s}}^d)_{n,\bar{t}}, \quad (2)$$

i.e., the importance scores assigned to features and timestamps are *relatively inconsistent* among overlapping time windows. The phenomenon is illustrated in Figure 1. The distribution of colors in the saliency maps represents the importance of the timestamps and input variables. The different cuts of the time windows (second row of

plots in Figure 1) are characterized by different color distributions than the original saliency map in the first row.

3.2 Robustness

Although similarly structured, we mentioned that images and time series intrinsically include a different semantic meaning due to the time dependency. However, the time series explanation should be insensitive to the feature ordering. A saliency explanation is considered as *robust* if the saliency changes accordingly when the features are swapped. We define the feature swapping operation on data window w_s^d and observe the effect in the corresponding saliency explanation S_s^d . Concretely, we swap random pair of features X_i and X_j ($i \neq j$) in w_s^d for all timestamps from t_s to t_{s+d-1} . Their feature attribution in S_s^d are $(S_s^d)_i$ and $(S_s^d)_j$. After features swapping, the data window is denoted by w_s^{*d} , and the newly learned saliency explanation is S_s^{*d} . $(S_s^d)_i$ corresponds to $(S_s^{*d})_j$ while $(S_s^d)_j$ corresponds to $(S_s^{*d})_i$. The saliency explanations are robust if $t_1, t_2 \in w_s^d \cap w_s^{*d}$ such that

$$(S_s^d)_{i,t_1} > (S_s^d)_{i,t_2} \text{ and } (S_s^{*d})_{j,t_1} > (S_s^{*d})_{j,t_2}, \quad (3)$$

i.e., important feature-time pixels maintain relative importance after swapping the feature of the data window. The phenomenon is illustrated in Figure 2.

4 EXPERIMENTS

We perform experiments on time series classification on real-world datasets. We generate various types of explanations in the form of saliency maps for the predictions made by the model to examine their consistency and robustness. We incorporate artificial padding into the input sequences to precisely control the feature importance and simulate the sliding window mechanism commonly used in time series analysis tasks. This section presents our findings on identifying inconsistency and non-robust saliency explanations across multiple datasets.

4.1 Datasets

We consider five real-world univariate time series datasets: *Power Demand* (PD), *Wine* (WIN), *Italy Power Demand* (IPD), *Two Lead ECG* (ECG) and *Mote Strain* (MS). PD derives from Keogh et al. [12], while the others are available in the UCR Archive [4].

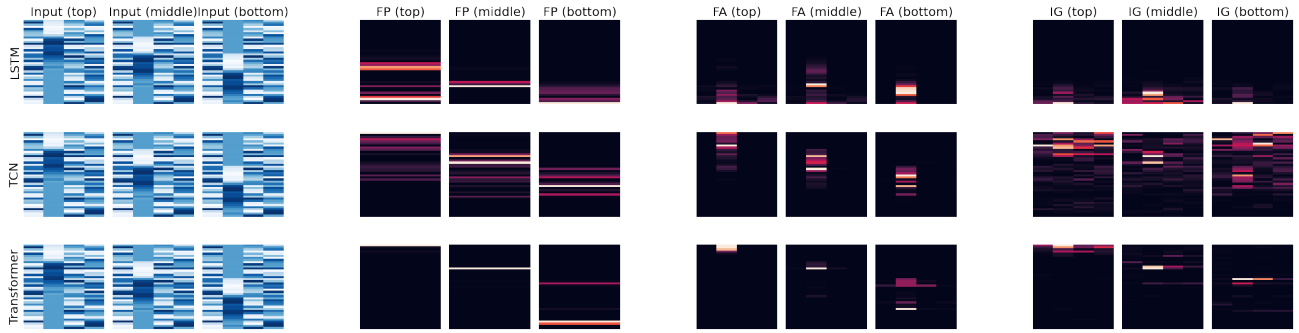


Figure 3: Saliency explanation of one data window from the IPD dataset: The leftmost group in blue heatmaps denotes the variants of one input frame from the IPD dataset, where rows are timestamps and columns are features. The real data window is located in the frame’s top, middle, and bottom third, and the rest elements are random noise. The saliency maps on the right side are acquired from three feature attribution algorithms: Feature Permutation (FP), Feature Ablation (FA), and Integrated Gradient (IG).

We preprocess all datasets by dividing them into non-overlapping windows a priori, and the class labels of each window are available. However, the ground truth data does not include the attribution of the prediction. In Sections 4.3 and 4.4, we introduce artificial padding with random noise to each input window and assign equal importance to the area of the original input.

4.2 Experimental setup

For our experiments, we select three representatives from the common saliency explanation approaches [8] for time series data. We employ *Feature Permutation* (FP) and *Feature Ablation* (FA) [25], which are perturbation-based methods, and *Integrated Gradients* (IG) [24], which is a gradient-based method. We use the implementation provided by Ismail et al. [8].

We investigate the behavior of saliency explanations on three types of network structures Recurrent Neural Networks (RNNs), Convolutional Neural Networks (CNNs), and attention-based networks. To this end, we picked three implementations commonly used for time series data: LSTM [7], TCN [13], and Transformer [27]. We configure these models with a Softmax output layer for classification and train the models on all the padded variants of the input windows, including top, middle and bottom padding. During the test phase, we generate saliency maps and analyze the effect of each group of padding variants separately.

4.3 Consistency evaluation

We apply artificial padding to each univariate time window to evaluate the explanation consistency over sliding windows. Specifically, we expand each univariate data window $w_s^d \in \mathbb{R}^{n \times d}$ to a matrix $m \in \mathbb{R}^{\alpha \times \lfloor \beta \cdot d \rfloor}$ ($\alpha > m$, $1 < \beta < 3$). The data window w_s^d is placed on d consecutive dimensions of m , and the other dimensions are filled with randomly sampled noise from a normal distribution. The effect of a sliding window can be simulated by placing w_s^d at different rows in m . Specifically, we allocate w_s^d at the top, middle, and bottom third of m to generate three overlapping sliding windows, i.e., three variants of each input window. We call the area in the saliency map corresponding to the input window w_s^d , the *area of interest*.

We show the experimental results by setting $\alpha = 4$ and $\beta = \frac{5}{3}$. An example of the padded data window is shown in Figure 3.

The proposed construction we get that each padding variant group (top/middle/bottom) contains the same input window only located differently. To examine the consistency of the saliency explanations, we compare the feature ranking of the obtained attributions in corresponding locations in each padding variant. As a showcase, we visualize the result of one window from the IPD dataset in Figure 3. The left three columns of Figure 3 represent the saliency explanations in the various padded input windows, the y -axis being the time and the x -axis being the input features. Only the second feature contains essential information to be learned by the classifiers (see the first column in Figure 3). The saliency maps on the right side correspond to the three explanation models FP, FA, and IG. We expect the second feature column’s top, middle, and bottom third to be marked as salient. However, as Ismail et al. [8] have already shown, classical saliency methods might fail on time series data due to the temporal feature, and our experiments confirm their results (see Figure 3) where the latest timestamps play more important roles in the prediction. The various explainers can detect the important timestamps and suffer from distinguishing important features for TCN and Transformers.

Despite the sub-optimal saliency explanations, we analyze the consistency between the padding variants. We evaluated the disagreement empirically on the saliency explanations using Kendall’s τ [11] and Pearson correlation; Kendall’s τ measures the smallest number of swaps of adjacent elements that transform one ranking into the other while the Pearson correlation coefficient measures the covariance of the two random variables divided by the product of their standard deviations. All quantities can be estimated using finite samples.

We calculate the importance scores for each timestamp and input feature, obtaining the importance ordering of the *area of interest*. For each pair of ranking from the three padding variants, we analyzed the pairwise comparisons among rankings of feature-time pixels in the saliency explanations FP, FA, and IG. The average Kendall’s τ and Pearson correlation (ρ) are summarized in Table 1 and the absolute values are visualized in Figure 4.

Table 1: Consistency ranking analysis

		Feature Permutation (FP)		Feature Ablation (FA)		Integrated Gradients (IG)	
		τ	ρ	τ	ρ	τ	ρ
PD	LSTM	0.936 ± 0.063	0.967 ± 0.035	0.868 ± 0.114	0.921 ± 0.092	0.852 ± 0.024	0.968 ± 0.012
	TCN	0.475 ± 0.143	0.625 ± 0.155	0.247 ± 0.200	0.334 ± 0.256	0.060 ± 0.148	0.080 ± 0.168
	Transformer	0.040 ± 0.136	0.049 ± 0.145	-0.049 ± 0.149	-0.086 ± 0.161	0.026 ± 0.138	0.030 ± 0.145
WIN	LSTM	0.914 ± 0.042	0.961 ± 0.023	0.843 ± 0.044	0.908 ± 0.030	0.918 ± 0.022	0.971 ± 0.009
	TCN	0.445 ± 0.164	0.530 ± 0.169	0.220 ± 0.159	0.287 ± 0.149	0.052 ± 0.200	0.057 ± 0.206
	Transformer	0.150 ± 0.192	0.196 ± 0.207	-0.11 ± 0.218	-0.198 ± 0.236	0.107 ± 0.180	0.140 ± 0.178
IPD	LSTM	0.475 ± 0.086	0.633 ± 0.101	0.531 ± 0.047	0.725 ± 0.045	0.767 ± 0.030	0.921 ± 0.019
	TCN	0.001 ± 0.083	-0.002 ± 0.112	-0.004 ± 0.075	-0.031 ± 0.095	0.192 ± 0.083	0.277 ± 0.114
	Transformer	0.124 ± 0.115	0.167 ± 0.157	0.054 ± 0.141	0.042 ± 0.199	0.204 ± 0.088	0.295 ± 0.121
ECG	LSTM	0.789 ± 0.070	0.873 ± 0.056	0.738 ± 0.062	0.827 ± 0.055	0.954 ± 0.007	0.995 ± 0.001
	TCN	0.102 ± 0.074	0.143 ± 0.096	0.072 ± 0.062	0.054 ± 0.070	0.129 ± 0.078	0.189 ± 0.101
	Transformer	0.089 ± 0.082	0.098 ± 0.110	0.020 ± 0.092	-0.038 ± 0.137	0.315 ± 0.066	0.453 ± 0.081
MS	LSTM	0.642 ± 0.072	0.768 ± 0.066	0.632 ± 0.078	0.753 ± 0.070	0.950 ± 0.007	0.995 ± 0.002
	TCN	0.038 ± 0.096	0.053 ± 0.134	-0.031 ± 0.116	-0.058 ± 0.167	0.055 ± 0.061	0.081 ± 0.089
	Transformer	0.124 ± 0.136	0.156 ± 0.189	0.093 ± 0.165	0.076 ± 0.244	0.291 ± 0.089	0.423 ± 0.125

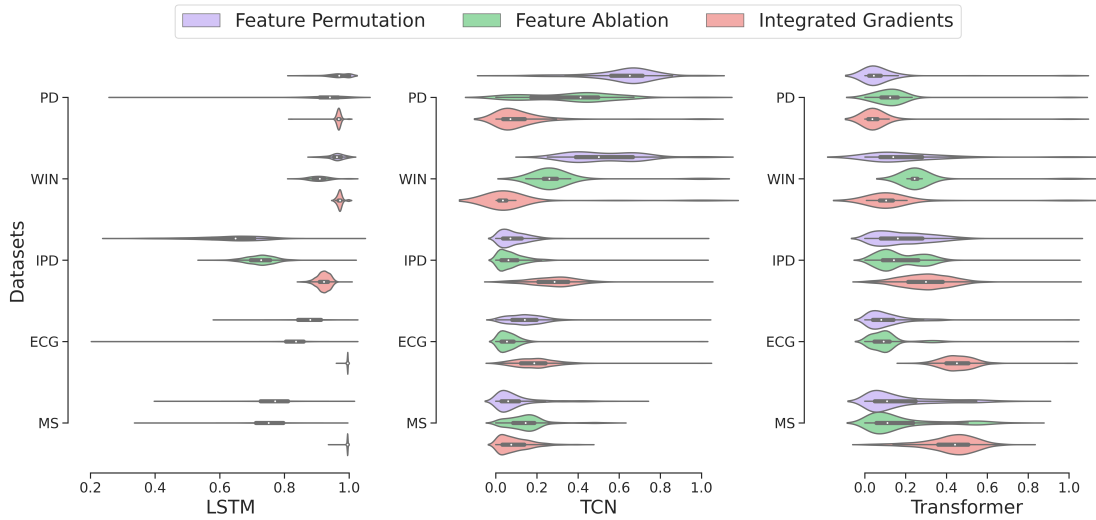
Table 2: Consistency Recall@k

		Feature Permutation (FP)			Feature Ablation (FA)			Integrated Gradients (IG)		
		Top	Middle	Bottom	Top	Middle	Bottom	Top	Middle	Bottom
PD	LSTM	0.041	0.000	0.000	0.072	0.000	0.000	0.165	0.268	0.268
	TCN	0.227	0.216	0.216	0.454	0.320	0.320	0.103	0.206	0.206
	Transformer	0.258	0.258	0.258	0.825	0.928	0.928	0.351	0.330	0.330
WIN	LSTM	0.064	0.051	0.051	0.103	0.060	0.060	0.244	0.248	0.248
	TCN	0.256	0.269	0.269	0.500	0.487	0.487	0.286	0.295	0.295
	Transformer	0.333	0.812	0.812	0.949	0.962	0.962	0.389	0.385	0.385
IPD	LSTM	0.250	0.250	0.250	0.625	0.708	0.708	0.375	0.458	0.458
	TCN	0.250	0.250	0.250	0.875	0.958	0.958	0.292	0.375	0.375
	Transformer	0.250	0.250	0.250	0.750	0.708	0.708	0.167	0.292	0.292
ECG	LSTM	0.171	0.171	0.171	0.341	0.244	0.244	0.256	0.268	0.268
	TCN	0.256	0.256	0.256	0.634	0.634	0.634	0.329	0.305	0.305
	Transformer	0.256	0.256	0.256	0.780	0.829	0.829	0.244	0.293	0.293
MS	LSTM	0.250	0.262	0.262	0.536	0.560	0.560	0.357	0.321	0.321
	TCN	0.250	0.262	0.262	0.750	0.798	0.798	0.298	0.381	0.381
	Transformer	0.250	0.250	0.250	0.845	0.821	0.821	0.274	0.369	0.369

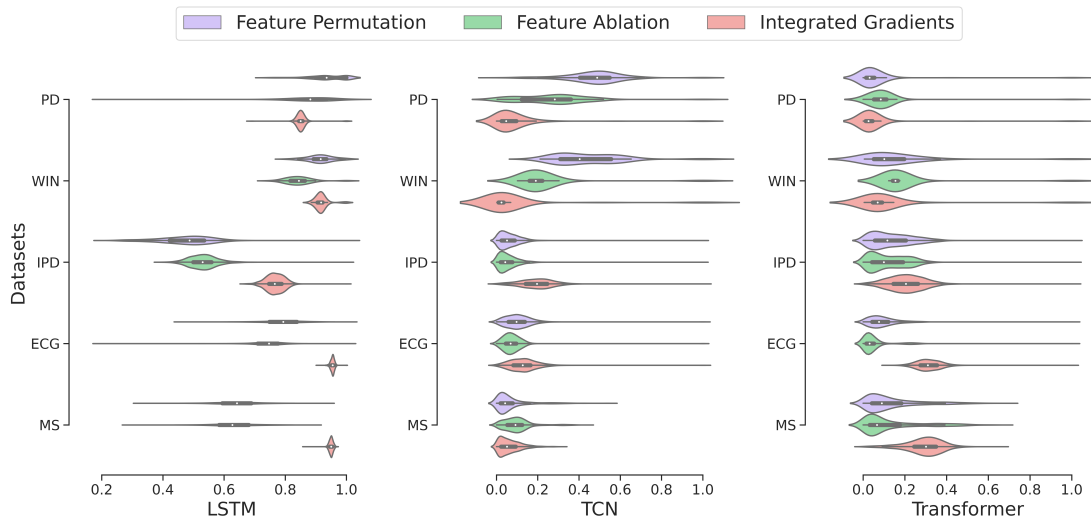
Table 1 contains, for each data set, neural network architecture, and saliency map, the average Kendall’s τ and Pearson correlation coefficients with the respective variance. From the table, it is easy to spot how the importance scores rankings provided vary in ranges below 1. Kendall’s τ and Pearson correlation coefficients range between 1 and -1 , where 1 indicates complete agreement among the rankings, while values close to zero suggest non-constant and independent orderings. From Figures 4a and 4b, we observe that the coefficients are, in most cases, crowded at low values, and episodes

of perfect agreement among the obtained rankings in the different windows are rare (although non-anomalies).

A special case is the LSTM algorithm that provides consistent saliency maps among the various windows. However, observing the explanation over the LSTM model, we see that both Kendall’s τ and Pearson correlation coefficients tend to accumulate to high scores (≈ 1) as the LSTM method tends to accumulate the learning in the last timestamps, thus implying that the explanation methods assign high importance only to the last timestamps. We further observe



(a) Violin plots of Pearson correlation absolute value



(b) Violin plots of Kendall's tau absolute value

Figure 4: Each row contains three plots (from left to right, LSTM, TCN, and Transformer architecture), while the colors code for the various explanation methods. Although the two metrics measure something essentially different, the behavior observed in (a) and (b) is similar.

FA correctly finds the relevant timestamps but cannot distinguish between noisy and relevant features.

In addition to the relative ranking, we also check the quality of the saliency explanation using $\text{Recall}@k$. Table 2 contains the $\text{Recall}@k$ obtained among the importance rankings of timestamps in the *areas of interest*. $\text{Recall}@k$ measures the ratio among correctly relevant and retrieved elements and the number of relevant elements and ranges in $[0, 1]$. High recall (≈ 1) indicates that the highly ranked feature-time pixels are concentrated in the area of interest, while low $\text{Recall}@k$ indicates the inability to find relevant elements correctly.

4.4 Robustness evaluation

To evaluate the robustness of the saliency explanation, we apply the feature swapping depicted in Figure 2. Specifically, we continue using the padded input matrix $m \in \mathbb{R}^{\alpha \times [\beta \cdot d]}$ from Section 4.3 and swap the feature dimensions containing the original input data window (*area of interest*) with noise dimensions. We train different classification models with the swapped and not swapped data. For simplicity, we always locate the original window in the middle of the selected feature dimension in this experiment. We compare the ranking of feature-time pixel explanations in the *areas of interest*

Table 3: Robustness ranking analysis

		Feature Permutation (FP)		Feature Ablation (FA)		Integrated Gradients (IG)	
		τ	ρ	τ	ρ	τ	ρ
PD	LSTM	0.972 ± 0.064	0.985 ± 0.036	0.973 ± 0.112	0.982 ± 0.102	0.807 ± 0.064	0.942 ± 0.066
	TCN	0.680 ± 0.168	0.803 ± 0.157	0.597 ± 0.259	0.706 ± 0.285	0.221 ± 0.148	0.307 ± 0.175
	Transformer	0.042 ± 0.141	0.052 ± 0.153	0.129 ± 0.148	0.164 ± 0.161	0.123 ± 0.133	0.171 ± 0.143
WIN	LSTM	0.932 ± 0.047	0.971 ± 0.021	0.924 ± 0.056	0.967 ± 0.029	0.929 ± 0.075	0.972 ± 0.057
	TCN	0.598 ± 0.107	0.696 ± 0.083	0.553 ± 0.094	0.676 ± 0.073	0.083 ± 0.186	0.105 ± 0.189
	Transformer	0.267 ± 0.241	0.347 ± 0.283	0.466 ± 0.153	0.587 ± 0.167	0.345 ± 0.149	0.473 ± 0.143
IPD	LSTM	0.446 ± 0.124	0.603 ± 0.147	0.579 ± 0.075	0.732 ± 0.076	0.699 ± 0.062	0.864 ± 0.053
	TCN	0.114 ± 0.141	0.157 ± 0.188	0.277 ± 0.159	0.358 ± 0.194	0.254 ± 0.137	0.361 ± 0.183
	Transformer	0.369 ± 0.158	0.480 ± 0.178	0.364 ± 0.215	0.458 ± 0.244	0.322 ± 0.148	0.449 ± 0.192
ECG	LSTM	0.821 ± 0.100	0.898 ± 0.073	0.841 ± 0.133	0.905 ± 0.103	0.967 ± 0.029	0.996 ± 0.028
	TCN	0.382 ± 0.119	0.515 ± 0.138	0.517 ± 0.087	0.657 ± 0.101	0.207 ± 0.125	0.300 ± 0.172
	Transformer	0.276 ± 0.126	0.365 ± 0.153	0.535 ± 0.141	0.673 ± 0.141	0.415 ± 0.081	0.582 ± 0.101
MS	LSTM	0.747 ± 0.112	0.857 ± 0.089	0.694 ± 0.107	0.811 ± 0.090	0.968 ± 0.027	0.996 ± 0.024
	TCN	0.147 ± 0.140	0.201 ± 0.187	0.184 ± 0.144	0.248 ± 0.189	0.068 ± 0.087	0.100 ± 0.126
	Transformer	0.473 ± 0.220	0.575 ± 0.238	0.513 ± 0.215	0.627 ± 0.239	0.453 ± 0.105	0.621 ± 0.125

Table 4: Robustness Recall@k

		Feature Permutation (FP)			Feature Ablation (FA)			Integrated Gradients (IG)		
		Top	Middle	Bottom	Top	Middle	Bottom	Top	Middle	Bottom
PD	LSTM	0.031	0.000	0.000	0.072	0.000	0.000	0.134	0.237	0.237
	TCN	0.227	0.258	0.258	0.299	0.443	0.443	0.155	0.216	0.216
	Transformer	0.268	0.309	0.309	0.742	0.876	0.876	0.268	0.299	0.299
WIN	LSTM	0.056	0.030	0.030	0.103	0.051	0.051	0.231	0.248	0.248
	TCN	0.274	0.265	0.265	0.389	0.355	0.355	0.295	0.282	0.282
	Transformer	0.303	0.252	0.252	0.466	0.568	0.568	0.179	0.372	0.372
IPD	LSTM	0.250	0.250	0.250	0.458	0.417	0.417	0.375	0.458	0.458
	TCN	0.250	0.250	0.250	0.458	0.500	0.500	0.333	0.375	0.375
	Transformer	0.250	0.250	0.250	0.458	0.542	0.542	0.292	0.333	0.333
ECG	LSTM	0.244	0.134	0.134	0.341	0.232	0.232	0.256	0.280	0.280
	TCN	0.256	0.256	0.256	0.476	0.476	0.476	0.232	0.256	0.256
	Transformer	0.256	0.256	0.256	0.634	0.622	0.622	0.390	0.305	0.305
MS	LSTM	0.250	0.250	0.250	0.381	0.417	0.417	0.333	0.262	0.262
	TCN	0.250	0.250	0.250	0.500	0.500	0.500	0.405	0.381	0.381
	Transformer	0.250	0.250	0.250	0.357	0.405	0.405	0.190	0.226	0.226

of swapped and not swapped pairs. The Kendall’s τ and Pearson correlation ρ are summarized in Table 3.

The absolute values of Kendall’s τ and Pearson correlation for TCN and Transformers indicate a significant difference in saliency maps after the swapping. In other words, when the important feature is switched with a noisy feature, the feature attribution in the saliency map is not switched correspondingly. An exception is the LSTM classifier, which explains all datasets except IPD robustly. However, the explanation quality is limited.

5 CONCLUSIONS

While explanations based on saliency maps have succeeded in vision and natural language domains, they remain still challenging for time series data. In addition to the well-known challenges posed by the additional time dimension to the input features, we have also identified issues related to *consistency* and *robustness*.

We exploited both the issue of *inconsistency* raising in saliency explanation over overlapping time windows and the issue of *non-robustness* when swapping features in time series windows. The

presented exploratory analysis aims to raise awareness of the described problems and motivates further development of saliency methods that address the existing flaws.

ACKNOWLEDGMENTS

This research was supported by the research training group *Dataninja* funded by the German federal state of North Rhine-Westphalia and by the Research Center Trustworthy Data Science and Security, an institution of the University Alliance Ruhr.

REFERENCES

- [1] Sebastian Bach, Alexander Binder, Grégoire Montavon, Frederick Klauschen, Klaus-Robert Müller, and Wojciech Samek. 2015. On pixel-wise explanations for non-linear classifier decisions by layer-wise relevance propagation. *PLoS one* 10, 7 (2015), e0130140.
- [2] David Baehrens, Timon Schroeter, Stefan Harmeling, Motoaki Kawanabe, Katja Hansen, and Klaus-Robert Müller. 2010. How to explain individual classification decisions. *The Journal of Machine Learning Research* 11 (2010), 1803–1831.
- [3] João Bento, Pedro Saleiro, André F Cruz, Mário AT Figueiredo, and Pedro Bizarro. 2021. Timeshap: Explaining recurrent models through sequence perturbations. In *Proceedings of the 27th ACM SIGKDD Conference on Knowledge Discovery & Data Mining*. 2565–2573.
- [4] Yanping Chen, Eamonn Keogh, Bing Hu, Nurjahan Begum, Anthony Bagnall, Abdullah Mueen, and Gustavo Batista. 2015. The UCR Time Series Classification Archive. www.cs.ucr.edu/~eamonn/time_series_data/.
- [5] Edward Choi, Mohammad Taha Bahadori, Jimeng Sun, Joshua Kulas, Andy Schuetz, and Walter Stewart. 2016. Retain: An interpretable predictive model for healthcare using reverse time attention mechanism. *Advances in neural information processing systems* 29 (2016).
- [6] Ann-Kathrin Dombrowski, Maximilian Alber, Christopher Anders, Marcel Ackermann, Klaus-Robert Müller, and Pan Kessel. 2019. Explanations can be manipulated and geometry is to blame. *Advances in neural information processing systems* 32 (2019).
- [7] Sepp Hochreiter and Jürgen Schmidhuber. 1997. Long short-term memory. *Neural computation* 9, 8 (1997), 1735–1780.
- [8] Aya Abdelsalam Ismail, Mohamed Gunady, Hector Corrada Bravo, and Soheil Feizi. 2020. Benchmarking deep learning interpretability in time series predictions. *Advances in neural information processing systems* 33 (2020), 6441–6452.
- [9] Sarthak Jain and Byron C. Wallace. 2019. Attention is not Explanation. *CoRR* abs/1902.10186 (2019). [arXiv:1902.10186](https://arxiv.org/abs/1902.10186) <http://arxiv.org/abs/1902.10186>
- [10] Deepak A Kaji, John R Zech, Jun S Kim, Samuel K Cho, Neha S Dangayach, Anthony B Costa, and Eric K Oermann. 2019. An attention based deep learning model of clinical events in the intensive care unit. *PLoS one* 14, 2 (2019), e0211057.
- [11] Maurice George Kendall. 1948. Rank correlation methods. (1948).
- [12] Eamonn Keogh, Jessica Lin, and Ada Fu. 2005. Hot sax: Efficiently finding the most unusual time series subsequence. In *Fifth IEEE International Conference on Data Mining (ICDM'05)*. Ieee, 8–pp.
- [13] Colin Lea, Michael D Flynn, Rene Vidal, Austin Reiter, and Gregory D Hager. 2017. Temporal convolutional networks for action segmentation and detection. In *proceedings of the IEEE Conference on Computer Vision and Pattern Recognition*. 156–165.
- [14] Scott M. Lundberg and Su-In Lee. 2017. A Unified Approach to Interpreting Model Predictions. In *NIPS*.
- [15] Qingyi Pan, Wenbo Hu, and Ning Chen. 2021. Two Birds with One Stone: Series Saliency for Accurate and Interpretable Multivariate Time Series Forecasting. In *IJCAI*. 2884–2891.
- [16] Vipin Pillai, Soroush Abbasi Koohpayegani, Ashley Ouligian, Dennis Fong, and Hamed Pirsiavash. 2022. Consistent Explanations by Contrastive Learning. In *Proceedings of the IEEE/CVF Conference on Computer Vision and Pattern Recognition*. 10213–10222.
- [17] Marco Tulio Ribeiro, Sameer Singh, and Carlos Guestrin. 2016. "Why should I trust you?" Explaining the predictions of any classifier. In *KDD*.
- [18] Chris Russell. 2019. Efficient search for diverse coherent explanations. In *Proceedings of the Conference on Fairness, Accountability, and Transparency*. 20–28.
- [19] Udo Schlegel, Hiba Amout, Mennatallah El-Assady, Daniela Oelke, and Daniel A Keim. 2019. Towards a rigorous evaluation of XAI methods on time series. In *2019 IEEE/CVF International Conference on Computer Vision Workshop (ICCVW)*. IEEE, 4197–4201.
- [20] Avanti Shrikumar, Peyton Greenside, and Anshul Kundaje. 2017. Learning important features through propagating activation differences. In *International conference on machine learning*. PMLR, 3145–3153.
- [21] Daniel Smilkov, Nikhil Thorat, Been Kim, Fernanda Viégas, and Martin Wattenberg. 2017. Smoothgrad: removing noise by adding noise. *arXiv preprint arXiv:1706.03825* (2017).
- [22] Huan Song, Deepta Rajan, Jayaraman Thiagarajan, and Andreas Spanias. 2018. Attend and diagnose: Clinical time series analysis using attention models. In *Proceedings of the AAAI conference on artificial intelligence*, Vol. 32.
- [23] Erik Strumbelj and Igor Kononenko. 2010. An Efficient Explanation of Individual Classifications Using Game Theory. *J Mach Learn Res* (2010).
- [24] Mukund Sundararajan, Ankur Taly, and Qiqi Yan. 2017. Axiomatic attribution for deep networks. In *International conference on machine learning*. PMLR, 3319–3328.
- [25] Harini Suresh, Nathan Hunt, Alistair Johnson, Leo Anthony Celi, Peter Szolovits, and Marzyeh Ghassemi. 2017. Clinical intervention prediction and understanding using deep networks. *arXiv preprint arXiv:1705.08498* (2017).
- [26] Che-Ping Tsai, Chih-Kuan Yeh, and Pradeep Ravikumar. 2022. Faith-shap: The faithful shapley shapley interaction index. *arXiv preprint arXiv:2203.00870* (2022).
- [27] Ashish Vaswani, Noam Shazeer, Niki Parmar, Jakob Uszkoreit, Llion Jones, Aidan N Gomez, Łukasz Kaiser, and Illia Polosukhin. 2017. Attention is all you need. *Advances in neural information processing systems* 30 (2017).
- [28] Matthew D Zeiler and Rob Fergus. 2014. Visualizing and understanding convolutional networks. In *ECCV*.
- [29] Yujia Zhang, Kuangyan Song, Yiming Sun, Sarah Tan, and Madeleine Udell. 2019. "Why Should You Trust My Explanation?" Understanding Uncertainty in LIME Explanations. *arXiv preprint arXiv:1904.12991* (2019).